

Similarity model for corner roll in turbulent Rayleigh-Bénard convection

Wen-Feng Zhou¹ and Jun Chen^{1, a)}

State Key Laboratory for Turbulence and Complex Systems
Department of Mechanics, College of Engineering, Peking University, Beijing 100871,
China

(Dated: 25 June 2019)

The corner-roll in the Rayleigh-Bénard convection accounts for the behaviors of heat transport and convection flow. Streamlines of the three-dimensional direct numerical simulations for $10^8 < Ra < 5 \times 10^9$ show that CR presents well-defined similarity and multi-layer structure. A stream function for CR is developed by homotopy and the structure ensemble dynamics. The model presents the scaling of Reynolds number of corner-roll $Re_{cr} \sim Ra^{1/4}$. Scaling of CR scale $r = 0.77Ra^{-0.085}$ indicates strong near-wall shearing induced by wind and provides a probability of the ‘ultimate regime’ at high Ra .

PACS numbers: 47.55.pb, 47.27.-i, 44.25.+f, 47.27.E-

The Rayleigh-Bénard (RB) convection is generated in a cell filled with fluid which is cooled from the top plate and heated from the bottom plate. The control parameters of an RB system are the Rayleigh number $Ra = \alpha g \Delta L_z^3 / (\kappa \nu)$ and the Prandtl number $Pr = \nu / \kappa$ of the fluid, and the aspect ratio $\Gamma = L_x / L_z$, where g is the gravitational acceleration, α the thermal expansion coefficient, ν the kinematic viscosity, and κ the thermal diffusivity, L_x and L_z are the dimensions of the cell in width and height directions, respectively. The response parameters are the Nusselt number, $Nu = q / [-\kappa(\partial T / \partial z)]$ and the Reynolds number, $Re = UL / \nu$.

The corner roll (CR) is the secondary flow at the corners of an RB cell, induced by the large-scale-circulation (LSC). Usually found in experiments¹⁻³ and numerical simulations⁴⁻⁶, the CR as a quasi-steady structure at the corner persistently contributes to heat transfer for high Ra number, despite Pr^7 . Some authors suggested that the local heat transfer coefficient (or the local Nu number) for the CR is larger than that in the shear region^{8,9}, being explained as the result of strong fluctuation and strong vorticity carried by CR with cool jet from cooling plate impinging on the heated wall¹⁰. In this sense, it is worthwhile to quantify the spatial structure of the CR and its heat transfer performance with a mathematical model. Some evidence indicates that the scale of CR decreases as increasing Ra . Thus investigating the behavior of CR also provide a way to explore the physics of the ultimate regime predicted by Kraichnan¹¹ in 1962.

Some researches have attempted to study the CR-type flow based on its properties. For high Re number cases, Batchelor¹² first proved that, under the steady Euler limit, for two-dimensional enclosed by vortex sheets, the vorticity away from the sheets is constant. Blythe et al.¹³ generalized this work to fluid with body force. For moderate Re number, Burggraf¹⁴ found that when $Re > 100$, the vortex develops from completely viscous to inviscid rotational core. They also derived that under Euler limit, the temperature in the core is uniform. For small Re number, Moffatt¹⁵ found a series of similarity solutions using separation variable method solving the Stokes

flow. He found that for the right angle, any flow sufficiently near the corner must consist of a sequence of eddies decreasing their size and intensity. In mathematical modelling of CR, Batchelor¹² and Burggraf¹⁴ proposed the analytical solutions by assuming the circular shape of the CR. However, the conditions for the solutions limit their application to the flow with complex configurations, e.g. the corner region in the RB convection. A solution for small Re number was suggested by Moffatt¹⁵, but it still cannot be directly applied to an RB cell either in the corner region of relatively high Re number or high Ra number. Therefore, it is necessary to develop a model to describe the CR in turbulent convection.

The SED theory claims that there are three kinds of basic ansatz in turbulent boundary layer (BL), i.e. power law, defect power law and generalized invariant relation by Lie group analysis¹⁶. Having been examined by canonical wall-bounded turbulence^{17,18}, the SED also unifies the temperature profile and the Ra -scaling of coefficient of the log-law¹⁹. In applications, the SED has been extended to develop turbulent transition model and RANS model for the flow around foils considering the effects of pressure gradient and finite Re number²⁰. Being invoked by the geometric similarity of the corner flow and the SED theory, we here developed a self-similarity model for CR based on SED and homotopy analysis.

We performed the 3D DNS for $Ra = 10^8, 5 \times 10^8, 10^9, 5 \times 10^9$ with $Pr = 0.7$ of the Boussinesq equations using a second-order staggered finite difference scheme from Verzicco and Orlandi²¹. The flow is confined in a narrow rectangular cell with aspect ratio of L_x (width) : L_y (depth) : L_z (height) = 1 : 1/6 : 1. The periodic boundary condition is employed in the depth (y) direction, and the large-scale convection flow is thus held on the xz -plane. The resolution of the simulations is up to $1024 \times 256 \times 800$ by clustering grid points near the boundaries. The largest grid scale is still smaller than the Kolmogorov and Batchelor scales^{22,23}, ensuring that both momentum and thermal energy are well resolved. The scaling of Nu of the DNS is $Nu = 3.27Ra^{0.294}$, consistent with other DNS and experiments^{24,25}.

Since no reversal of LSC occurs through the computational time and the quasi-steady CRs are held at the corners of the cell, the statistical properties of CR are obtained by time-average of flow field, which are shown in Fig. 1(a). The triangular CRs

^{a)}Electronic mail: jun@pku.edu.cn

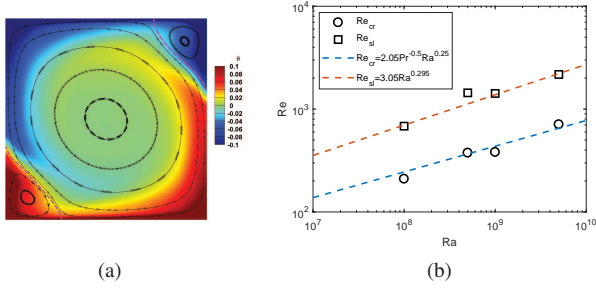


FIG. 1: (a) Time-average field colored by temperature for $Ra = 1 \times 10^8$. The arrowed-lines represent the streamline. The purple dashed lines mark the slip lines. (b) The Ra -scaling of Re of CR, slip line, represented by symbols. The blue line is the CR scaling given by the model. The black line is the empirical fitting of the slip line scaling. The red line is the correlation of CR and the slip line.

are wedged at the corners along the diagonal direction of the cell. The slip line as the interface between CR and LSC playing a key role in transporting kinetic energy between the large-scale structures. In statistical sense, the energy sustaining rotating of a CR is supported both by shearing of slip line from LSC and the buoyancy from horizontal conducting plate.

It is seen that the Ra number has limited effect on the triangle-shaped CR, the scale of which diminishes with increasing Ra . The velocity on the slip line reaches its maximum in the middle with zero velocity at both stagnation ends. Particularly, the maximum velocity in the middle of the slip line implies local intensive momentum and energy transport between CR and LSC, which decreases with increasing Ra . To quantify the momentum transfer ability of the slip line, we define the Reynolds number of the slip line as $Re_{sl} = \int \frac{v_{sl} l}{\nu} dl$, where v_{sl} is the average velocity on slip line and l the length of slip line, representing a scaling law of Ra , $Re_{sl} = 3.15Ra^{0.295}$; see Fig. 1(b).

A model based on the circumferential similarity of the streamlines inside CR is developed. An algorithmic expression of the streamlines is obtained by *homotopy*, giving the transformation expression of two formula continuously deforming from one to another²⁶. We here construct a homotopy $H : X \times I \rightarrow Y, I = [0, 1]$ for any $f \in X, H(f, 0) = f_2$ and $H(f, 1) = f_1$, where $f_2(x, z) = 0$ represents a small vicinity of the CR center, and $f_1(x, z) = 0$ is the function of the CR boundary. When $\xi \in I$ as the similarity variable changes from 0 to 1, $f(x, z) = 0$ for $H(f, \xi) = 0$ deforms continuously from $f_2(x, z) = 0$ to $f_1(x, z) = 0$.

The implicit homotopy expression is simplified by linearly combining f_1 and f_2 , $H = \xi f_1 + (1 - \xi)\Lambda_0 f_2$. If $H = 0$, we get the explicit form of ξ as

$$\xi = \Lambda_0 f_2 / (-f_1 + \Lambda_0 f_2) \quad (1)$$

where Λ_0 is considered as the constraint strength between the inner and outer layer.

The least square procedure is used to obtain f_1 , f_2 and the magnitude Λ_0 . The boundary of CR, f_1 , is composed of two

walls and the slip line. To keep accuracy, the slip line is expressed as a cubic function $z - (a + bx + cx^2 + dx^3) = 0$. The walls are respectively written as $x = 0$ and $z = 0$. Thus the boundary of CR is given as $f_1 = -xz(z - (a + bx + cx^2 + dx^3)) = 0$. On the other hand, the inner boundary as a small core at the central region of CR is expressed as $f_2 = (x - s_0)^2 + (z - t_0)^2 - \epsilon^2 = 0$, where (s_0, t_0) is the coordinates of the center, and ϵ the radius of the core. In the case of $Ra = 10^8$, they are $a = 0.36, b = -1, 955, c = 10.07, d = -29.58, s_0 = 0.11, t_0 = 0.11, \epsilon = 0.0001$. The strength factor Λ_0 in the range of $[0.05, 0.2]$ (e.g. $\Lambda_0 = 0.12$ for $Ra = 1 \times 10^8$) indicates that, for the present cases, the constraint of the rigid wall is always stronger than that of the center.

We consider independent similarity variable ξ (Eq. (1)) and the stream function ψ as the dependent similarity variable. The dimensionless Reynolds-averaged Navier-Stokes (RANS) equations can be written as

$$u_i \partial_i u_j = -\partial_j p + Ra^{-1/2} Pr^{1/2} \partial_{ii} u_j - \partial_i \overline{u_j u_i} + \theta \delta_{j3}, \quad (2)$$

where u_j, p, θ represent the Reynolds-average quantities. The velocity component is expressed in the stream-function form, using $u_1 = \partial \psi / \partial z, u_3 = -\partial \psi / \partial x$. Then we have

$$A = V + \Pi, \quad (3)$$

where $A = \partial_3 \psi \partial_{ii} \partial_1 \psi - \partial_1 \psi \partial_{ii} \partial_3 \psi$ is advection term, $V = Ra^{-1/2} Pr^{1/2} \partial_{ii} \partial_{jj} \psi$ is viscous term and $\Pi = \partial_{13} (\overline{u'_3 u'_3} - \overline{u'_1 u'_1}) + \partial_{11} \overline{u'_1 u'_3} - \partial_{33} \overline{u'_1 u'_3} - \partial_1 \theta$ is fluctuation term.

As discussed above, the viscosity effect on CR is relatively small and negligible. Thus, the balance is $A \approx \Pi$. Based on the geometry similarity, we assume that stream function has a similarity solution under the similarity variable ξ , i.e. $\psi = \psi[\xi] = \psi[x, y; a_0]$, and have

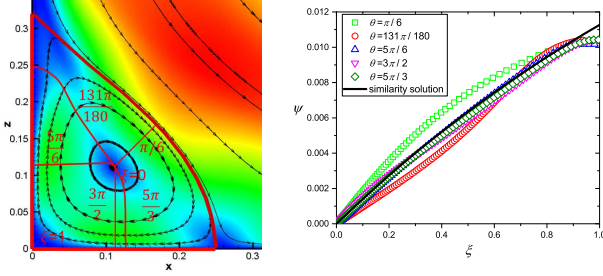
$$\psi_\xi (\psi_{\xi\xi} h_1 + \psi_\xi h_2) = \Pi, \quad (4)$$

where $h_1 = 2[\partial_1 \xi \partial_3 \xi \partial_{11} \xi + (\partial_3 \xi)^2 \partial_{13} \xi - (\partial_1 \xi)^2 \partial_{13} \xi - \partial_1 \xi \partial_3 \xi \partial_{33} \xi]$ and $h_2 = \partial_{111} \xi \partial_3 \xi + \partial_{133} \xi \partial_3 \xi - \partial_{113} \xi \partial_1 \xi - \partial_{333} \xi \partial_1 \xi$, representing the coordinate transformation functions. A similarity solution requires Π to be a function of ξ , i.e. $\Pi = \Pi(\xi)$, and the ratio of $h_2/h_1 = c_2$ is a constant or a function of ξ .

The DNS show that the viscosity effect on CR is so weak that negligible. Thus a relationship between the fluctuation terms and the stream-function-differential term ψ_ξ is established as $\Pi/\psi_\xi^2 = c_1$. We have $\psi_\xi [\psi_{\xi\xi} + \psi_\xi (c_1 + c_2)] = 0$ with its solution $\psi = \psi_0 \exp(-\xi/\xi_0) + B$, where $\xi_0 = 1/(c_1 + c_2)$. Considering the inner boundary condition $\psi(\xi = 0) = 0$, then the stream-function follows

$$\psi = \psi_0 \left(1 - e^{-\xi/\xi_0}\right), \quad (5)$$

as an exact similarity solution. The coefficients ψ_0 and ξ_0 can be measured from DNS (e.g. $\psi_0 = 0.028, \xi_0 = 1.9429$ for $Ra = 1 \times 10^8$). By analyzing the stream function profiles along the similarity coordinate ξ at different central angles, one can see that the stream function collapses well to the DNS, except



(a) The CR colored by the magnitude of velocity. (b) Stream function profile for the angles marked in Fig. 2(a).

FIG. 2: The CR and its stream function profiles at five angles for the case of $Ra = 10^8$.

for the profile of angle of $\pi/6$. Eq. (5) is the solution of the flow under the solid wall condition, thus the profile near the slip line has a perceptible deviation.

The stream function for the bulk is no longer proper for the near-wall flow — viscosity should be taken into account. Canonical turbulent BL theory cannot successfully describe the undeveloped flow in CR. Moreover, the fluid near the wall being advected downstream undergoes the varying pressure gradient along with emission of thermal plumes. To obtain a function of boundary layer (BL) in CR, we apply the structure ensemble dynamics (SED) theory¹⁶, by introducing the stress length and the symmetry of the wall taking into account the constraint of solid wall, pressure gradient, and thermal effects¹⁹.

Space average of the momentum equation in the steamwise direction and integration from 0 to z gives

$$\frac{du^+}{dz^+} - \frac{\overline{u'w'}}{u_\tau^2} = 1 + \frac{1}{u_\tau^2 L_z} \int_0^z (p_r - p_l) dz, \quad (6)$$

where u and $u'w'$ are steamwise-average variable and p_r and p_l are the right and left side wall pressure, respectively. Velocity and length scale are normalized by friction velocity $u_\tau = \sqrt{\nu du/dz|_{z=0}}$ and viscous length $l_\nu = \nu/u_\tau$. By introducing $S^+ = \frac{du^+}{dz^+}$, $W^+ = -\frac{\overline{u'w'}}{u_\tau^2}$, $\tau^+ = 1 + \frac{1}{u_\tau^2 L_z} \int_0^z (p_r - p_l) dz$, we have $S^+ + W^+ = \tau^+$. In the region near the wall, $\tau^+ \approx 1$. Substituting the stress length function $\ell_M^+ = \sqrt{W^+}/S^+$ as the multilayer similarity function of the BL gives

$$S^+ = \left(-1 + \sqrt{1 + 4\ell_M^{+2}\tau^+} \right) / (2\ell_M^{+2}). \quad (7)$$

The velocity profile is eventually obtained by integrating from 0 to z , $u = u_\tau u^+ = u_\tau \int_0^z S^+ dz$.

We apply SED to quantify the pressure gradient effect on BL in CR. The stress length along x direction is $\ell_{M,x}^+ = \sqrt{W_x^+}/S_x^+$ for the horizontal BL and the stress length in z direction $\ell_{M,z}^+ = \sqrt{W_z^+}/S_z^+$ for the vertical BL. We apply Taylor expansion to the shear rate S^+ and the Reynolds stress W^+ . The no-slip boundary and continuity condition follow $u \sim z$, $w \sim z^2$ for horizontal BL. We have $\ell_{M,x}^+ = \sqrt{W_x^+}/S_x^+ = \ell_{0,x} z^{3/2}$ for

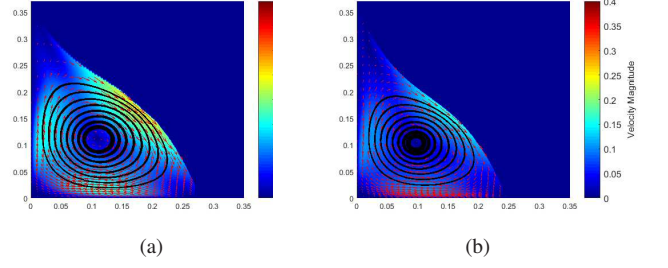


FIG. 3: Comparison of DNS with reconstruction of the similarity solution. Velocity magnitude nephogram and vector arrow represent the DNS and the steam-line is obtained from Eq. (5) (a) $Ra = 1 \times 10^8$; (b) $Ra = 10^9$

the BL. Similarly, the stress length of vertical BL is $\ell_{M,z}^+ = \sqrt{W_z^+}/S_z^+ = \ell_{0,z}(x^+)^{3/2}$, where $\ell_{0,x}$ and $\ell_{0,z}$ are the coefficient and the function of x or z , respectively. The parameter $\ell_{0,x}$ is expressed as follows

$$\ell_{0,x} = \begin{cases} a_1(x - x_0), & 0 < x < x_c \\ b_1/(x_{ap} - x), & x_c < x < x_{ap} \end{cases} \quad (8)$$

where x_0 ($0.01 < x_0 < 0.0533$ for the present study) is the critical point defining the two ranges; x_c ($0.0747 < x_c < 0.11$) the position of the core of CR for different Ra numbers. The parameters, a_1 ($2.35 < a_1 < 4.5$), $b_1 (= 0.4Ra^{-0.125})$, x_{ap} ($0.19 < x_{ap} < 0.26$) are related to Ra number. Similarly, $\ell_{0,z}$ can be expressed as

$$\ell_{0,z} = \begin{cases} b_3/z, & 0 < z < z_c \\ a_3(z_0 - z), & z_c < z < z_0, \end{cases} \quad (9)$$

where z_0 ($0.206 < z_0 < 0.2692$ for the present study) is the position of the separation point, z_c ($0.0819 < z_c < 0.11$) is the position of the core of CR. The parameters, $a_3 (= 500Ra^{-0.28})$ and $b_3 (= 1.3Ra^{-0.2})$ are determined by Ra number. It is noteworthy that the relations between the parameters and Ra number, i.e. x_0 , x_c , a_1 , x_{ap} , z_0 and z_c as the functions of Ra , cannot be determined with the present simulated cases. Further simulations with wider range of Ra are necessary to obtain the parameters in the stress lengths. Combining the stream function for the bulk and the multi-layer structure for the BL, we have a unified model for CR. $\ell_{0,x}$ and $\ell_{0,z}$ indicate that the eddy scale is inversely proportional to the upstream distance with favorable pressure gradient and decreases linearly with adverse pressure gradient.

Comparison of the model-reconstructed CR and the DNS, we find that the streamlines and velocity distribution are almost the same except for those very close to the core and the slip line. At the core, low Reynolds effect might cause the elliptical core. The slip line is expressed in Eq. (1), which does not specify the difference between the solid wall and the slip line, though the solid wall has stronger constraint than the slip line. As an assessment of the model, the relative error is examined as 10.93% for $Ra = 1 \times 10^8$ and 10.45% for $Ra = 10^9$ — all below 11%.

The downwelling flow around the slip line is fully turbulence, and the CR is confined in the corner. As the heated bottom plate pumps energy into the corner region, enforcing the vorticity of CR. Thus, the scale of the CR varying with Ra is determined by these effects. The CR is characterized both by $|\psi_0/\xi_0|$, which is $\psi_0/\xi_0 = 1.45Ra^{-1/4}$, and the scale of CR, r .

The scale of CR, r is defined as the average distance of the core to the intersection point of walls, which is found to obey the scaling law as $r = 0.77Ra^{-0.085}$. The negative power exponent indicates that high Ra would suppress the CR and thus elongate the wind shearing region. Recalling the conjecture of realization of ‘ultimate region’ induced by the fully turbulent BL^{11,27,28}, a relatively wilder shear region would improve turbulence of the BL^{29,30}. Therefore, the Reynolds number of CR is given as

$$Re_{cr,mod} = \frac{u_{cr,mod} r \cos \theta}{\nu} \simeq \frac{|\psi_0/\xi_0| \sqrt{Ra/Pr}}{C_1} \quad (10)$$

Using $r/L_z = 0.77Ra^{-0.085}$, $|\psi_0/\xi_0| = 1.45Ra^{-1/4}$ and $C_1 = 1/\sqrt{2}$, we have $Re_{cr,mod} = 1.45\sqrt{2}Ra^{1/4}Pr^{1/2}$. It is noted that although the characteristic velocity and scale become smaller at higher Ra , the solution of Moffatt for the Stokes flow of the corner cannot be applied either.

The heat transport in the corner roll region is investigated. Being invoked by the hypothesis of mixing zone³¹, we obtained the correlation between Re_{cr} and Nu_{cr} . The assumptions are listed as follows: (a) The characteristic velocity of CR fulfils an anomalous scaling as $u_{cr} \sim (\alpha g \Delta_{cr} L)^{1/2} Ra^\chi$; (b) temperature scale of the bulk of CR is proportional to the temperature difference of the top and bottom plate, i.e. $\Delta_{cr}/\Delta \sim const.$; (c) heat flux is determined by the inner convection heat transport, $H \sim u_{cr} \Delta_{cr}$; (d) w_h is of the same order of the CR’s characteristic velocity, i.e. $u_{cr} \sim w_h$; (e) during the emission of plumes, viscous force and buoyancy are balanced as $\alpha g \Delta \sim \nu w_h / \lambda_{cr}^2$; (f) defining a number of scaling indexes through the relations $Re_{cr} = \frac{u_{cr} r}{\nu} \sim Ra^\epsilon$, $Nu_{cr}^{-1} = \lambda_{cr} / L_z \sim \frac{\kappa \Delta / L_z}{H} \sim Ra^{-\beta}$, $\frac{r}{L_z} \sim Ra^\eta$. Based on relations of (a), (b) and (f), we have

$$\frac{u_{cr} r}{\nu} \sim \left(\frac{\alpha g \Delta L_z^3}{\kappa \nu} \right)^{1/2} \left(\frac{\kappa}{\nu} \right)^{1/2} Ra^\chi \frac{r}{L_z}. \quad (11)$$

Relations of (c) and (f) follow

$$\frac{u_{cr} r}{\nu} \frac{\nu}{\kappa} \frac{L_z}{r} \sim Ra^\beta. \quad (12)$$

Relations of (d), (e) and (f) give

$$\frac{u_{cr} r}{\nu} \sim \frac{\alpha g \Delta L_z^3}{\kappa \nu} \frac{\lambda_{cr}^2}{L_z^2} \frac{\kappa}{\nu} \frac{r}{L_z}. \quad (13)$$

The power exponents in Eq. (11) – (13) give

$$\begin{cases} \epsilon = 1/2 + \chi + \eta \\ \beta = \epsilon - \eta \\ \epsilon = 1 - 2\beta + \eta \end{cases}. \quad (14)$$

With the scaling of CR scale $\eta = -0.085$, we get the rest exponents, which are $\beta = 1/3$, $\epsilon = 1/3 - \eta = 0.248$, and

$\chi = 1/3 - 1/2 = -1/6 \approx -0.167$. The DNS show that the scalings of the characteristic velocity $u_{cr}/U_f \sim Ra^{-0.165}$, and that of Reynolds number $Re_{cr} = \frac{u_{cr} r}{\nu} \sim Ra^{0.250}$, close to the scalings from the assumptions. More importantly, the thermal boundary thickness described by the approximation is $\lambda_{cr}/L \sim Ra^{-1/3}$, in agreement with the DNS, $\lambda_{cr,dns}/L_z \sim Ra^{-0.331}$. It is noteworthy that the assumption of the constant CR temperature has only been examined with the unit aspect ratio. The validity of the assumption at different aspect ratios needs further investigation.

The present results can be extended to the large scale circulation. While we established the stream function for corner roll, it is likely that the stream-function for the boundary for the triangular shape of the corner roll but also applicable for the hexagon boundary of the bulk flow; see Fig. 1(a). Another important aspect is the multilayer structure of the vertical and horizontal profiles near the walls. We anticipate that, depending on the boundary type, the boundary layer of the large-scale circulation may be described by the similar multilayer function, in particular for the solid wall boundary, and for the slip line.

Another intriguing question relates to the assumptions specified for the CR, in relation to the Re number. The positive scaling of Re_{cr} ($\epsilon = 0.248$) indicates that the corner roll is enforced by increasing the Ra number, though the size of CR decreases with the Ra number with a negative exponent $\eta = -0.085$. The enhancement of convection leads intensive heat transport at higher Ra number, i.e. $Nu \sim Ra^{0.331}$, where the power exponent even higher than in the wind shearing region ($Nu \sim Ra^{0.295}$).

From the hypothesis building perspective, our work also motivates investigating separation scenarios leading to enhanced heat transport. In the future, we also plan to explore parameterization of the streamline functions of CR and bulk flow. Finally, it may prove fruitful for more detailed simulations to study the corner roll under various control parameters, such as the PrR number, Γ .

We thank Zhen-Su She for helpful comments and suggestions. This work is supported by National Nature Science (China) Fund 11452002, 11521091, and 11372362, and by MOST (China) 973 project 2009CB724100.

¹Ruby Krishnamurti and Louis N Howard. Large-scale flow generation in turbulent convection. *Proceedings of the National Academy of Sciences*, 78(4), 1981.

²Xin-Liang Qiu and Ke-Qing Xia. Spatial structure of the viscous boundary layer in turbulent convection. *Physical Review E*, 58(5):5816, 1998.

³JJ Niemela, L Skrbek, KR Sreenivasan, and RJ Donnelly. The wind in confined thermal convection. *Journal of Fluid Mechanics*, 449:169–178, 2001.

⁴Roberto Benzi and Roberto Verzicco. Numerical simulations of flow reversal in rayleigh-bénard convection. *EPL (Europhysics Letters)*, 81(6):64008, 2008.

⁵Kazuyasu Sugiyama, Enrico Calzavarini, Siegfried Grossmann, and Detlef Lohse. Flow organization in two-dimensional non-oberbeck-boussinesq rayleigh-bénard convection in water. *Journal of Fluid Mechanics*, 637:105–135, 2009.

⁶Nan Shi, Mohammad S Emran, and Jörg Schumacher. Boundary layer structure in turbulent rayleigh-bénard convection. *Journal of Fluid Mechanics*, 706:5–33, 2012.

⁷Sebastian Wagner, Olga Shishkina, and Claus Wagner. Boundary layers and

- wind in cylindrical rayleigh-bénard cells. *Journal of Fluid Mechanics*, 697: 336–366, 2012.
- ⁸Robert Kaiser and Ronald du Puits. Local wall heat flux in confined thermal convection. *International Journal of Heat and Mass Transfer*, 73:752–760, 2014.
- ⁹Ronald du Puits, Ling Li, Christian Resagk, André Thess, and Christian Willert. Turbulent boundary layer in high rayleigh number convection in air. *Physical review letters*, 112(12):124301, 2014.
- ¹⁰Ronald du Puits and Christian Willert. The evolution of the boundary layer in turbulent rayleigh-bénard convection in air. *Physics of Fluids*, 28(4): 044108, 2016.
- ¹¹Robert H Kraichnan. Turbulent thermal convection at arbitrary prandtl number. *The Physics of Fluids*, 5(11):1374–1389, 1962.
- ¹²Go K Batchelor. On steady laminar flow with closed streamlines at large reynolds number. *Journal of Fluid Mechanics*, 1(02):177–190, 1956.
- ¹³PA Blythe, A Liakopoulos, and E Haçuta. Thermally driven flows at low prandtl numbers: An extension of the prandtl-batchelor theorem. *International journal of engineering science*, 33(12):1699–1711, 1995.
- ¹⁴Odu R Burggraf. Analytical and numerical studies of the structure of steady separated flows. *Journal of Fluid Mechanics*, 24(01):113–151, 1966.
- ¹⁵HK Moffatt. Viscous and resistive eddies near a sharp corner. *Journal of Fluid Mechanics*, 18(01):1–18, 1964.
- ¹⁶Zhen-Su She, Xi Chen, and Fazle Hussain. Quantifying wall turbulence via a symmetry approach: a lie group theory. *Journal of Fluid Mechanics*, 827: 322–356, 2017. doi:10.1017/jfm.2017.464.
- ¹⁷Xi Chen, Fazle Hussain, and Zhen-Su She. Bulk flow scaling for turbulent channel and pipe flows. *EPL (Europhysics Letters)*, 115(3):34001, 2016.
- ¹⁸Bin Wu, Weitao Bi, Fazle Hussain, and Zhen-Su She. On the invariant mean velocity profile for compressible turbulent boundary layers. *Journal of Turbulence*, 18(2):186–202, 2017.
- ¹⁹Zhen-Su She, Xi Chen, Hong-Yue Zou, Yun Bao, Jun Chen, and Fazle Hussain. Prediction of temperature distribution in turbulent rayleigh-benard convection. *arXiv preprint arXiv:1401.2138*, 2014.
- ²⁰Meng-Juan Xiao and Zhen-Su She. A new algebraic transition model based on stress length function. In *APS Meeting Abstracts*, 2016.
- ²¹R Verzicco and Paolo Orlandi. A finite-difference scheme for three-dimensional incompressible flows in cylindrical coordinates. *Journal of Computational Physics*, 123(2):402–414, 1996.
- ²²Olga Shishkina, Richard JAM Stevens, Siegfried Grossmann, and Detlef Lohse. Boundary layer structure in turbulent thermal convection and its consequences for the required numerical resolution. *New Journal of Physics*, 12(7):075022, 2010.
- ²³Richard JAM Stevens, Roberto Verzicco, and Detlef Lohse. Radial boundary layer structure and nusselt number in rayleigh-bénard convection. *Journal of fluid mechanics*, 643:495–507, 2010.
- ²⁴Guenter Ahlers, Siegfried Grossmann, and Detlef Lohse. Heat transfer and large scale dynamics in turbulent rayleigh-bénard convection. *Reviews of modern physics*, 81(2):503, 2009.
- ²⁵F Chillà and J Schumacher. New perspectives in turbulent rayleigh-bénard convection. *The European Physical Journal E: Soft Matter and Biological Physics*, 35(7):1–25, 2012.
- ²⁶Shijun Liao. *Beyond perturbation: introduction to the homotopy analysis method*. CRC press, 2003.
- ²⁷Siegfried Grossmann and Detlef Lohse. Scaling in thermal convection: a unifying theory. *Journal of Fluid Mechanics*, 407:27–56, 2000.
- ²⁸Siegfried Grossmann and Detlef Lohse. Multiple scaling in the ultimate regime of thermal convection. *Physics of Fluids*, 23(4):045108, 2011.
- ²⁹Walter Tollmien. über die entstehung der turbulenz. In *Vorträge aus dem Gebiete der Aerodynamik und verwandter Gebiete*, pages 18–21. Springer, 1930.
- ³⁰Hermann Schlichting. Zur entstehung der turbulenz bei der plattenströmung. *Nachrichten von der Gesellschaft der Wissenschaften zu Göttingen, Mathematisch-Physikalische Klasse*, 1933:181–208, 1933.
- ³¹Bernard Castaing, Gemunu Gunaratne, François Heslot, Leo Kadanoff, Albert Libchaber, Stefan Thomae, Xiao-Zhong Wu, Stéphane Zaleski, and Gianluigi Zanetti. Scaling of hard thermal turbulence in rayleigh-bénard convection. *Journal of Fluid Mechanics*, 204:1–30, 1989.